Available online at www.sciencedirect.com
SCIENCE DIRECT®
International Journal of Heat and Mass Transfer 47 (2004) 3047–3055
International Journal of HEAT and MASS TRANSFER
www.elsevier.com/locate/ijhmt

Macrosegregation during alloyed semiconductor crystal growth in strong axial and transverse magnetic fields

Martin V. Farrell, Nancy Ma *

Department of Mechanical and Aerospace Engineering, North Carolina State University, Campus Box 7910, Raleigh, NC 27695, USA

Received 23 July 2003; received in revised form 28 February 2004
Available online 17 April 2004

Abstract

This paper presents a model for the unsteady species transport during bulk growth of alloyed semiconductor crystals with both axial and transverse magnetic fields. During growth of alloyed semiconductors such as germanium–silicon (GeSi) and mercury–cadmium–telluride (HgCdTe), the solute's concentration is not small so that density differences in the melt are very large. These compositional variations drive compositionally-driven buoyant convection, or solutal convection, in addition to thermally-driven buoyant convection. These buoyant convections drive convective transport which produce non-uniformities in the concentration in both the melt and the crystal. This transient model predicts the distribution of species in the entire crystal grown in a magnetic field. The present study investigates the effects of magnetic field orientation and strength on the segregation in alloyed semiconductor crystals, and presents results of concentration in the crystal and in the melt at several different times during crystal growth.
© 2004 Elsevier Ltd. All rights reserved.

1. Introduction

During alloyed semiconductor crystal growth without a magnetic field, oscillatory melt motions produce undesirable spatial oscillations of the concentration in the crystal. Since molten semiconductors are excellent electrical conductors, an externally-applied magnetic field can be used to control their melt motion and species transport in order to optimize the species distribution during the growth process. The infinite number of possible magnetic field configurations, namely, field strengths and orientations, provides the ability to tailor the melt motion in order to optimize the properties of the crystal. An externally-applied magnetic field is used to create a body force which provides an electromagnetic (EM) damping of the melt motion and to eliminate oscillations in the melt motion and thus in the composition of the crystal. Unfortunately, the elimination of mixing and a moderate EM damping of the residual melt motion may lead to a large variation of the crystal's composition in the direction perpendicular to the growth direction (lateral or radial macrosegregation).

If the EM damping is extremely strong, then the melt motion is suppressed and has no effect on the composition in the crystal, then this diffusion-controlled species transport may produce a laterally and axially uniform composition in the crystal except in the first-grown and last-grown parts of the crystal [1]. In order to achieve diffusion-controlled species transport, the species transport Péclet number $Pe_m = U_c L/D$ must be small, where U_c is the characteristic velocity for the magnetically-damped melt motion and is inversely proportional to the square of the magnetic flux density B_0, while L is the characteristic dimension of the melt and D is the diffusion coefficient for the species in the molten semiconductor. If $Pe_m \ll 1$, then the characteristic ratio of convection to diffusion of the species is small and the species transport is diffusion controlled. However, since typical values of D are $1–2 \times 10^{-8}$ m^2/s, B_0 must be extremely large for diffusion-controlled species transport on Earth [2]. Therefore, the objective is to identify a

* Corresponding author. Tel.: +1-919-515-5231; fax: +1-919-515-7968.
E-mail address: nancy_ma@ncsu.edu (N. Ma).

0017-9310/$ - see front matter © 2004 Elsevier Ltd. All rights reserved.
doi:10.1016/j.ijheatmasstransfer.2004.02.021

moderate field which is strong enough to eliminate flow oscillations but which only moderately damps the residual melt motion in order to achieve both lateral and axial compositional uniformity in the crystal. Recently, Garandet and Alboussière [3] reviewed the literature on modelling and experimental studies of Bridgman growth in a magnetic field, while Walker [4] reviewed the use of asymptotic methods in modelling of melt motion, heat transfer and species transport during crystal growth with steady magnetic fields.

During the Bridgman growth of alloyed semiconductor crystals, the application of magnetic fields have shown great promise. For example, Watring and Lehoczky [5] have shown that the radial variation between the maximum and minimum concentrations can be decreased by more than a factor of three with the application of a 5 T magnetic field, arising because the magnetic field retards the sinking of the heavier melt to the center of the ampoule, resulting in less radial segregation. Ramachandran and Watring [6] reported a reduction in the radial segregation in all of their samples which were grown in a magnetic field.

For alloyed semiconductors, the density differences due to compositional variations in the melt are very large. In germanium–silicon (GeSi), for example, the mole fraction of germanium may vary from 0.95 in the melt which has not yet received any rejected germanium to 0.99 near the interface, and this compositional difference corresponds to a density difference of nearly 300 kg/m^3. In a frequently used extension of the Boussinesq approximation, the melt density is assumed to vary linearly with both the temperature and mole fraction of either species. In this approximation, the magnitudes of the density difference and of the resultant buoyant convection associated with the temperature variation or with the compositional variation are characterized by $\beta_t(\Delta T)_0$ and $\beta_c C_0$, respectively, where β_t and β_c are the thermal and compositional coefficients of volumetric expansion, while $(\Delta T)_0$ and C_0 are the characteristic radial temperature difference and the initially uniform mole fraction of the species, i.e. of silicon in the GeSi melt. For GeSi with $(\Delta T)_0 = 10$ K and $C_0 = 0.06$, the characteristic ratio of the buoyant convection driven by thermal variations to that driven by compositional variations is $\beta_t(\Delta T)_0/\beta_c C_0 = 0.0667$. While the thermally-driven buoyant convection is probably not negligible, particularly far from the crystal-melt interface where compositional variations are small, the compositionally-driven buoyant convection or solutal convection is dominant particularly near the interface. Garandet et al. [7] investigated the effects of a tranverse magnetic field on buoyant convection in a rectangular container while Farrell and Ma [8] investigated the effects of an axial magnetic field.

In a previous study [9], we presented an asymptotic and numerical solution for the dilute species transport during the solidification of a GeSi crystal with both axial and transverse magnetic fields. This study only considered pure crystals with very small dopant concentrations so that there was only thermally-driven buoyant convection, where the velocity and temperature were independent of the dopant concentration and known at each time step, and the governing equation for species conservation was a linear equation with known spatially variable coefficients given by an analytical solution for velocity. During growth of alloyed semiconductor crystals, the velocity and mole fraction of either species are intrinsically coupled because the buoyant convection is driven by both thermal and compositional variations in the melt. In the 1970s, Hart [10] presented an asymptotic and numerical solution for the motion of a stratified salt solution with both thermally-driven and compositionally-driven buoyant convection and without a magnetic field or solidification. In a recent study [11], we treated both thermally-driven and compositionally-driven buoyant convection during the solidification of an alloyed GeSi crystal with an axial magnetic field. In the present paper, we extend this study [11] to treat these phenomena during growth with a transverse magnetic field and investigate the effect of the magnetic field orientation. Several crystal growers are currently performing experiments on the Bridgman growth of germanium crystals with various amounts of silicon and with strong magnetic fields [3,12]. We use a two-dimensional model problem in a horizontal container to develop an asymptotic method, to provide physical insight, and to investigate the effect of the magnetic field's orientation. Future research will extend this model to treat realistic systems such as vertical Bridgman and floating-zone crystal growth processes.

2. Problem formulation

We treat the unsteady, two-dimensional species transport of a species in a solidifying, electrically-conducting semiconductor melt in a horizontal, rectangular container with thermally insulated top and bottom walls and with an externally applied, uniform, steady horizontal (axial) magnetic field $B_0\hat{\mathbf{x}}$ or vertical (transverse) magnetic field $B_0\hat{\mathbf{y}}$. Here, B_0 is the magnetic flux density, while $\hat{\mathbf{x}}, \hat{\mathbf{y}}$, and $\hat{\mathbf{z}}$ are the unit vectors for the Cartesian coordinate system. The coordinates and lengths are normalized by half the distance between the top and bottom walls L, and a is the dimensionless length of the container. The constant uniform heat flux q into the right end of the container keeps the semiconductor molten. The heat flux removed at the left end of the container is adjusted so that the crystal-melt interface moves at a constant velocity $U_g = \omega U_c$, where ω is the dimensionless interface velocity. With time t normalized by L/U_c, the dimensionless time to grow the entire crystal is a/ω.

Experiments [5] have shown that magnetic fields can control compositionally-driven buoyant convection so that the electromagnetic body force must be comparable to the characteristic gravitational body force associated with compositional variations. Since the electric currents only arise from the melt motions across the magnetic field, the magnetic field can damp the motion but cannot completely suppress it. Therefore, this balance gives a characteristic velocity for the magnetically-damped compositionally-driven buoyant convection,

$$U_c = \frac{\rho_0 g \beta_c C_0}{\sigma B^2} \tag{1}$$

where ρ_0 is the melt's density at the solidification temperature T_0, g is gravitational acceleration, and σ is the electrical conductivity of the melt. Thus we can expect the melt motion to decrease roughly as B_0^{-2} as the magnetic field strength is increased.

The electric current in the melt produces an induced magnetic field which is superimposed on the applied magnetic field produced by the external magnet. The characteristic ratio of the induced to the applied magnetic field strengths is the magnetic Reynolds number $R_m = \mu_p \sigma U_c L$, where μ_p is the magnetic permeability of the melt. For all crystal growth processes, $R_m \ll 1$ and the additional magnetic fields produced by the electric currents in the melt are negligible.

We assume that the temperature differences and compositional variations are sufficiently small that all the physical properties of the melt can be considered uniform and constant except for the density in the gravitational body force term of the Navier–Stokes equation. In this Boussinesq-like approximation, the characteristic temperature difference $(\Delta T)_0$ and the characteristic mole fraction difference $(\Delta C)_0$ are assumed to be sufficiently small that the melt's density is a linear function of temperature and composition, given by

$$\rho = \rho_0[1 - \beta_t(T^* - T_0) - \beta_c(C^* - C_0)], \tag{2}$$

and that $\beta_t(\Delta T)_0 \ll 1$ and $\beta_c(\Delta C)_0 \ll 1$, where T^* is the temperature in the melt and C^* is the mole fraction of one species in the melt.

The equations governing the melt motion, heat transfer and species transport are

$$N^{-1}\left[\frac{\partial \mathbf{v}}{\partial t} + (\mathbf{v}\cdot\nabla)\cdot\mathbf{v}\right] = -\nabla p + (\gamma T + C - 1)\hat{\mathbf{y}} + \mathbf{j}\times\mathbf{B} + Ha^{-2}\nabla^2\mathbf{v}, \tag{3a}$$

$$\nabla\cdot\mathbf{v} = 0, \quad \nabla\cdot\mathbf{j} = 0, \quad \mathbf{j} = -\nabla\phi + \mathbf{v}\times\mathbf{B}, \tag{3b, c, d}$$

$$Pe_t\left[\frac{\partial T}{\partial t} + (\mathbf{v}\cdot\nabla)T\right] = \nabla^2 T, \tag{3e}$$

$$Pe_m\left[\frac{\partial C}{\partial t} + (\mathbf{v}\cdot\nabla)C)\right] = \nabla^2 C, \tag{3f}$$

$$C = \frac{C^*}{C_0}, \quad T = \frac{T^* - T_0}{(\Delta T)_0}, \quad \gamma = \frac{\beta_t(\Delta T)_0}{\beta_c C_0}, \tag{3g, h, i}$$

where p is the deviation of the pressure from the hydrostatic pressure for the uniform density ρ_0 normalized by $\sigma U_c B_0^2 L$, ϕ is the electric current potential normalized by $U_c B_0 L$, T is the deviation of the dimensional melt's temperature from the solidification temperature normalized by $(\Delta T)_0$, C is the mole fraction normalized by its initially uniform value C_0 and $\mathbf{v} = u\hat{\mathbf{x}} + v\hat{\mathbf{y}}$ is the dimensionless velocity. Here, u and v are the horizontal and vertical velocities, respectively, normalized by U_c. In the Navier–Stokes Eq. (3a), $\mathbf{B}$ is equal to $\hat{\mathbf{x}}$ for the axial magnetic field or $\hat{\mathbf{y}}$ for the transverse magnetic field. The characteristic ratio of the EM body force to the inertial force is the interaction parameter $N = \sigma^2 B_0^4 L/\rho_0^2 g\beta_c C_0$. The square root of the characteristic ratio of the EM body force to the viscous force is the Hartmann number $Ha = B_0 L(\sigma/\mu)^{1/2}$. Eqs. (3b) and (3c) are continuity of mass and of electric current, respectively, while Eq. (3d) is Ohm's law. In conservation of energy given by Eq. (3e), the characteristic ratio of the convective to conductive heat transfer is the thermal Péclet number $Pe_t = \rho_0^2 g\beta_c C_0 c_p L/\ k\sigma B_0^2$, where c_p and k are the specific heat and the thermal conductivity of the melt, respectively. Eq. (3f) is conservation of species for the solute in the molten semiconductor. During the growth of a GeSi crystal for $C_0 = 0.06$ with $(\Delta T)_0 = 10$ K, $\gamma = 0.0667$. Under these conditions with a 2 T magnetic field, $U_c = 0.00050566$ m/s, $N = 21,574.2$, $Ha = 793.3$, $Pe_t = 0.3034$ and $Pe_m = 189.6$.

In our two-dimensional model problem, nothing varies in the z direction, and there can be a uniform electric field in the z direction E_z. In any actual horizontal Bridgman process, there are electrically insulating walls at, say, $z = \pm d$, which block any electric current in the z direction. For the present recirculating flow, $E_z = 0$ for zero net electric current. The electric current density normalized by $\sigma U_c B_0$, and Ohm's law gives $\mathbf{j} = -v\hat{\mathbf{z}}$ for the axial field, or $\mathbf{j} = u\hat{\mathbf{z}}$ for the transverse field.

For a sufficiently strong magnetic field, Pe_t is small, so that the convective heat transfer terms in Eq. (3e) are negligible. Ma and Walker [13] found that the error due to neglect of convective heat transfer is less than 4% for $Pe_t \leqslant 15.0$, so that convective heat transfer is certainly negligible for our present process with $Pe_t = 0.3034$. With negligible convective heat transfer, the crystal-melt interface is planar as shown in Fig. 1. In general, $U_g < U_c$, so that the heat released by the cooling melt is negligible compared to the conductive heat transfer [14]. Since the latent heat and convective heat transfer is negligible, the crystal-melt interface is planar and isothermal at the freezing temperature [14]. Therefore, the heat flux through the melt is uniform and constant, and the deviation of the melt's temperature from T_0, normalized by $Lq/k = (\Delta T)_0$, is

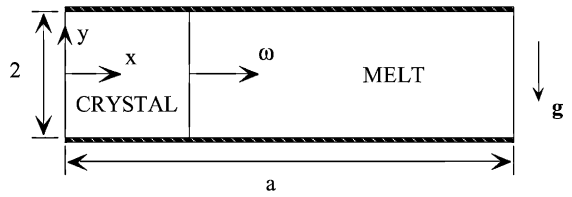

Fig. 1. Two-dimensional model problem with a uniform, steady axial magnetic field or transverse magnetic field $\mathbf{B} = \hat{\mathbf{x}}$ or $\mathbf{B} = \hat{\mathbf{y}}$, and with coordinates normalized by half the distance between the top and bottom walls.

$$T = x - \omega t. \tag{4}$$

In certain situations, Seebeck effects are very important [15]. However, in the present situation with strong magnetic fields, the thermoelectric current generated by the temperature gradient along the interfaces is negligible compared to the electric currents in the melt [16].

In the Navier–Stokes equation, inertial terms are negligible for a sufficiently strong magnetic field. In a recent study, Ma and Walker [13] found that the error due to the neglect of inertial effects is only 2.7% for $N = 16.59$, and is totally negligible for $N \geqslant 648.1$, so that inertial effects are certainly negligible for our present process with $N = 21,574.2$. In an asymptotic solution for $Ha \gg 1$ for our inertialess melt motion, the melt is divided into an inviscid core, Hartmann layers with $O(Ha^{-1})$ thickness, and parallel layers with $O(Ha^{-1/2})$ thickness. For the axial field $\mathbf{B} = \hat{\mathbf{x}}$, the Hartmann layers lie adjacent to the crystal-melt interface along $\xi = -1$ and the right end of the container along $\xi = +1$, while the parallel layers lie adjacent to the top and bottom walls at $y = \pm 1$. Here, $\xi = [2x - (a + \omega t)]/(a - \omega t)$ is our rescaled axial coordinate so that $-1 \leqslant \xi \leqslant +1$ for all time. For the transverse field $\mathbf{B} = \hat{\mathbf{y}}$, the Hartmann layers lie adjacent to the top and bottom walls, while the parallel layers lie adjacent to the crystal-melt interface and the right end of the container. The Hartmann layers carry an $O(Ha^{-1})$ flow that has a simple, local, exponential structure, which matches any core or parallel velocity, and which satisfies the no-slip conditions along the crystal-melt interface or container wall. While the Hartmann layers represent an extremely small fraction of the melt's volume and flowrate, the parallel layers occupy a significant fraction of the melt and carry an $O(Ha^{1/2})$ velocity. Therefore, a formal asymptotic analysis for $Ha \gg 1$ is not appropriate but the numerical solution of the inertialess Navier–Stokes equation with all the viscous terms is not necessary. Thus, we use a hybrid solution which does not assume that the parallel layer's thickness is small. This hybrid solution neglects the $O(Ha^{-1})$ volume flux deficiency in the Hartmann layers and the $O(Ha^{-1})$ perturbation in the parallel layers.

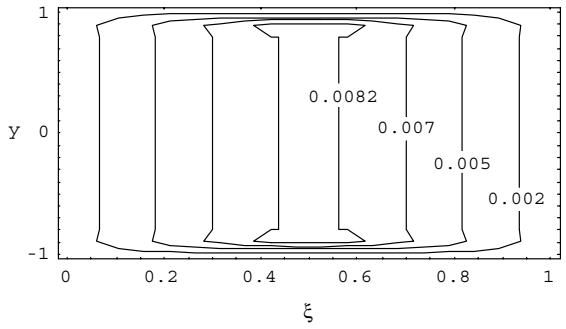

Fig. 2. Streamfunction in the melt at the beginning of growth $\psi(\xi, y, t = 0)$ for an axial magnetic field with $B_0 = 2$ T.

For the axial field $\mathbf{B} = \hat{\mathbf{x}}$, we discard the viscous terms $Ha^{-2}\partial^2\mathbf{v}/\partial x^2$ in the Navier–Stokes equation, and we relax the no-slip conditions at both $\xi = \pm 1$ because they are satisfied by the Hartmann layers which are not part of the hybrid solution. We apply the boundary conditions $u = 0$ along $\xi = \pm 1$, and we apply the no-slip and no-penetration conditions along $y = \pm 1$. At the beginning of growth with $a = 1$, the concentration in the melt is uniform and the melt motion is driven entirely by thermally-driven buoyant convection as shown in Fig. 2 for $B_0 = 2$ T and $C_0 = 0.06$. In Fig. 2, the maximum value of the streamfunction is 0.008599, where the streamfunction is

$$u = \frac{\partial \psi}{\partial y}, \quad v = -\frac{2}{a - \omega t}\frac{\partial \psi}{\partial \xi}, \tag{5a, b}$$

The hotter fluid near $\xi = +1$ flows vertically upward and flows to the left for $y > 0$. When the fluid reaches the colder end of the container near the crystal-melt interface, it flows vertically downward, and either solidifies or turns and flows to the right for $y < 0$.

For the transverse field $\mathbf{B} = \hat{\mathbf{y}}$, we discard the viscous terms $Ha^{-2}\partial^2\mathbf{v}/\partial y^2$ in the Navier–Stokes equation, and we relax the no-slip conditions at both $y = \pm 1$ because they are satisfied by the Hartmann layers which are not part of the hybrid solution. We apply the boundary conditions $\mathbf{v} = 0$ along $y = \pm 1$, and we apply the no-slip and no-penetration conditions along $\xi = \pm 1$. Since the core carries an $O(1)$ flow, the flow circuit must be completed through two high-velocity parallel layers with $u = O(1)$ and $v = O(Ha^{1/2})$ inside these layers at $\xi = \pm 1$, as reflected in the streamlines at the beginning of growth in Fig. 3 for $a = 1$, $B_0 = 2$ T and $C_0 = 0.06$. In Fig. 3, the maximum value of the streamfunction is 0.03418. Figs. 2 and 3 indicate that the flows are vastly different. With an axial field, there are $O(Ha^{1/2})$ velocity jets adjacent to the top and bottom walls at $y = \pm 1$ and an $O(1)$ flow adjacent to the crystal-melt interface. With a transverse field, the high-velocity fluid flows along the crystal-melt interface. The location of the $O(Ha^{1/2})$ flow has a sig-

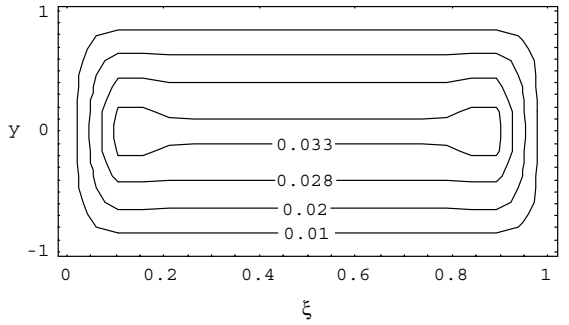

Fig. 3. Streamfunction in the melt at the beginning of growth $\psi(\xi, y, t = 0)$ for a transverse magnetic field with $B_0 = 2$ T.

nificant effect on the species transport in the melt, because the convection of solute is strong in the regions where there are high velocity flows.

For the species transport, the boundary condition at the crystal-melt interface is

$$\frac{\partial C}{\partial \xi} = -\frac{(a - \omega t)}{2} Pe_g (1 - k_s) C, \quad \text{at } \xi = -1, \tag{6}$$

where $Pe_g = U_g L/D = \omega Pe_m$ is the growth Péclet number. Along each of the other surfaces, there cannot be diffusion of species into the impermeable container, so that $\nabla C \cdot \hat{\mathbf{n}} = 0$, where $\hat{\mathbf{n}}$ is the unit normal vector.

At the beginning of crystal growth, the concentration of silicon, normalized with the initial uniform concentration, is $C(\xi, y, t = 0) = 1$. Thus the amount of silicon initially in the melt is obtained by integrating across the ampoule's volume giving a total dimensionless silicon concentration equal to $2a$. We verify that the sum of the total silicon in the melt and in the crystal is equal to $2a$ at each time step.

Assuming that there is no diffusion of species in the solid crystal, $C_s(x, y)$, normalized by the initial uniform concentration in the melt, is given by

$$C_s(x, y) = k_s C(\xi = -1, y, t = x/\omega), \tag{7}$$

where $k_s = 4.2$ for silicon in a germanium melt. Future research will investigate the effects of the solidification temperature and the segregation coefficient on concentration, where $T_0(C^*) = 938.3 + 1300C^* - 2100C^{*2} + 2056C^{*3} - 783C^{*4}$ and $k_s(C^*) = 4.2 - 8.7C^* + 6.0C^{*2} + 3.3C^{*3} - 3.8C^{*4}$, where T_0 is in °C [17].

We use a Chebyshev spectral collocation method for the spatial derivatives in the inertialess form of the Navier–Stokes Eq. (3a) with T given by Eq. (4) and for the spatial derivatives in species transport Eq. (3f) with Gauss-Lobatto collocation points in ξ and y. For the time derivative in Eq. (3f), we use a second-order implicit time integration scheme. We integrate from $t = 0$ to a t which is slightly less than a/ω. We use a large enough number of collocation points in each direction for both the streamfunction and concentration at each time step so that the velocity and concentration gradients are resolved, and a large enough number of time steps such that the results do not change by increasing the number of time steps. Forty one and 51 collocation points in the ξ and y directions, respectively, were sufficient to resolve the velocity and concentrations for the axial magnetic field. Eighty one and 33 collocation points in the ξ and y directions, respectively, were sufficient to resolve the velocity and concentration gradients for the transverse magnetic field. For both magnetic field orientations, 800 times steps were sufficient.

In the classical well-mixed limit, the rejected germanium is instantly uniformly mixed over the volume of the melt at each time. In this limit, the crystal composition is given by

$$C_s(x) = k_s \left(1 - \frac{x}{a}\right)^{-(1-k_s)}. \tag{8}$$

In the classical diffusion-controlled limit, the crystal concentration is uniform at the melt's initial uniform composition $C = 1$ everywhere except the first-grown and last-grown parts of the crystal. In the initial and final transients corresponding to the first-grown and last-grown parts of the crystal, respectively, the crystal compositions are given by exponential curves which are functions of k_s and Pe_g [1].

3. Results for growth in an axial magnetic field

We present results for the growth of a GeSi crystal in an axial magnetic field with $a = 1$, $U_g = 10$ μm/s, $C_0 = 0.06$, and $B_0 = 2$ T, for which $Pe_g = 3.75$, $\gamma = 0.0667$, $U_c = 0.00050566$ m/s, $Ha = 793.33$, $Pe_m = 189.62$, $\omega = 0.004944$, and $a/\omega = 50.566$.

Once crystal growth begins, the crystal absorbs silicon which creates a silicon-depleted region in the melt adjacent to the crystal-melt interface. At very early stages of growth, this concentration gradient is primarily axial and drives diffusion of silicon towards the interface. The melt motion adjacent to the bottom wall at $y = -1$ quickly carries the silicon away from the interface. After 2.5% of the crystal has grown at $t = 0.1264$, there is a small concentration gradient adjacent to the crystal-melt interface which produces a solutal convection that augments the thermal convection and which causes a small increase in the maximum value of the streamfunction from the initial value $\psi_{max} = 0.008599$ to 0.01025. The concentration is lowest at $\xi = -1$ and $y = -1$ because the interface absorbs silicon and because the vertically downward flow convects silicon-depleted flow toward this stagnation point, and the difference between the melt's concentration at $y = +1$ and $y = -1$ is $\Delta C = 0.00259$. At this time, the contours of the streamfunction nearly resemble those in Fig. 2 with a slight shift to the left because the streamfunction is no

longer symmetric about $\xi = 0$. As growth progresses, the combination of absorption of silicon at the interface and convection of silicon away from the interface reduces the average concentration in the melt. Therefore, the maximum value of the streamfunction decreases as growth progresses. After 20% of the crystal has grown at $t = 10.11$, the maximum value of the streamfunction is 0.04882, as reflected in the contours of the streamfunction presented in Fig. 4a. Adjacent to $y = -1$, the $O(Ha^{1/2})$ velocities produce a strong local flow which convects the silicon-depleted flow to the right. However, the concentration gradient is largest near the crystal-melt interface so that the circulation in Fig. 4a has moved towards the interface. Fig. 4a reflects a dominance of solutal convection as compared with the contours of the streamfunction presented at the beginning of growth in Fig. 2 in which the melt motion is driven entirely by thermal convection. At the time, the minimum and maximum values of the concentration in the melt have reduced to 0.1668 and 0.9998, respectively, as reflected in the constant-concentration curves in Fig. 4b. In Fig. 4b, the difference between the melt's concentration along the interface at $y = +1$ and $y = -1$ is $\Delta C = 0.5492$. When 30% of the crystal has grown at $t = 15.17$, this difference has become $\Delta C = 0.5939$. A formal asymptotic analysis reveals that the thicknesses of the parallel layers are actually $O\{[(a - \omega t)/Ha]^{1/2}\}$

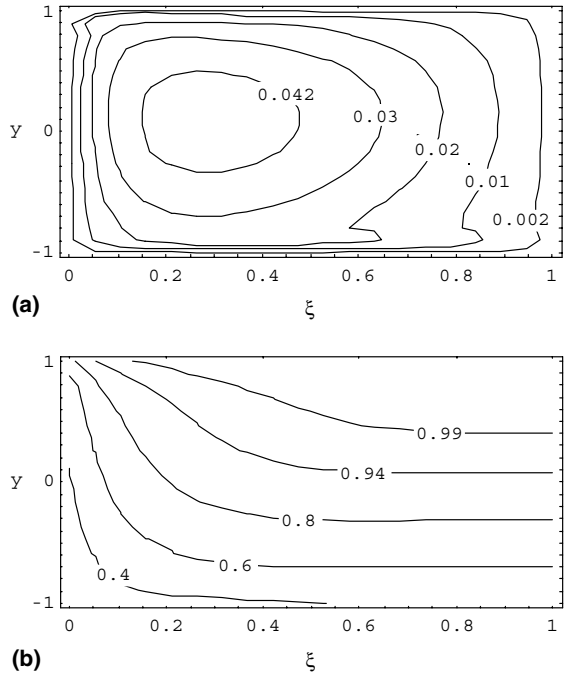

Fig. 4. Contours of the streamfunction and concentration in the melt at $t = 10.11$ for an axial magnetic field with $B_0 = 2$ T and $C_0 = 0.06$: (a) $\psi(\xi, y, 10.11)$, (b) $C(\xi, y, 10.11)$.

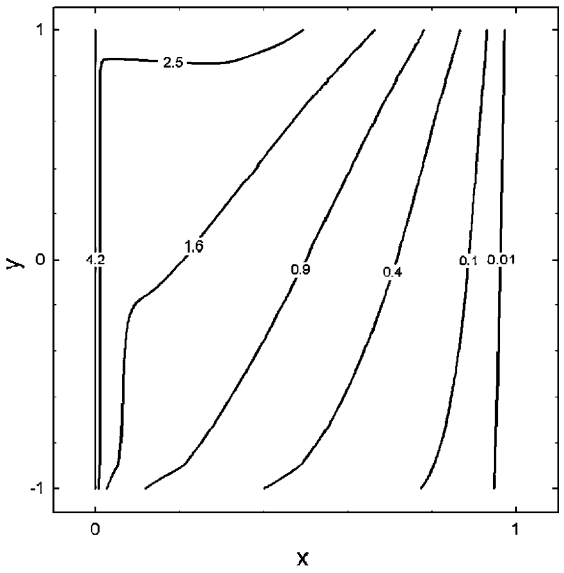

Fig. 5. Contours of the concentration in the crystal $C_s(x, y)$ for an axial magnetic field with $B_0 = 2$ T, $C_0 = 0.06$, $U_g = 10$ μm/s and $a = 1$.

and that the horizontal velocities inside the parallel layers adjacent to $y = \pm 1$ are actually $u = O\{[Ha/(a - \omega t)]^{1/2}\}$. Therefore, as growth progresses and the melt length decreases, the convection of the silicon-depleted melt away from the interface increases. After this time $t = 15.17$, the convection of silicon-depleted melt causes a decrease in ΔC. When 40% of the crystal has grown, this difference has reduced to $\Delta C = 0.5860$ and when 80% of the crystal has grown, this difference has further reduced to $\Delta C = 0.1668$, reflecting a decrease in the lateral segregation as crystal growth progresses.

The constant-concentration curves in the crystal are presented in Fig. 5. In Fig. 5, the first-grown part of the crystal solidifies with $C_s(0, y) = k_s = 4.2$. The concentration quickly decreases with x because the segregation coefficient is large. The concentration is lower near $y = -1$ than $y = +1$ because the large velocity in the parallel layer adjacent to the bottom wall quickly convects the silicon-depleted melt away from the crystal-melt interface. The decrease in the lateral segregation is reflected in Fig. 5 as the contours become more vertical as x increases.

4. Results for growth in a transverse magnetic field

We present results for the growth of a GeSi crystal in a transverse magnetic field with $a = 1$, $U_g = 10$ μm/s, $C_0 = 0.06$, and $B_0 = 2$ T, for which $Pe_g = 3.75$, $\gamma = 0.0667$, $U_c = 0.00050566$ m/s, $Ha = 793.33$, $Pe_m = 189.62$, $\omega = 0.004944$, and $a/\omega = 50.566$.

With a transverse field, the high-velocity $O(Ha^{-1/2})$ parallel layer adjacent to the crystal-melt interface at $\xi = -1$. After 2.5% of the crystal has grown at $t = 0.1264$, the maximum value of the streamfunction has dramatically increased from the initial value $\psi_{max} = 0.03418$ to 0.1194. The silicon-depleted melt has not had time to diffuse or convect away from the interface so that there is a strong circulation adjacent to the interface which is dominated by solutal convection as reflected in the contours of the streamfunction presented in Fig. 6. At this stage, the minimum and maximum values of the concentration in the melt are 0.8239 and 1.0, respectively, and the constant-concentration curves are vertical with a large axial gradient near the crystal-melt interface and most of the melt at the initial uniform concentration $C = 1$. After 20% of the crystal has grown at $t = 10.11$, the maximum value of the streamfunction is $\psi_{max} = 0.09290$ as shown in Fig. 7a. In Fig. 7a, the crowded contours of the streamfunction adjacent to the crystal-melt interface reflect the $O(Ha^{1/2})$ vertically downward velocities in the parallel layer. This strong vertically downward flow provides a strong convective species transport reflected in the sharpness of the constant-concentration curves adjacent to the crystal-melt in Fig. 7b. In Fig. 7a, the silicon-depleted melt has convected or diffused over the entire volume of the melt, and the minimum and maximum values of the concentration are 0.1270 and 0.9977, respectively. At this time, the difference between the concentration in the melt at $y = +1$ and $y = -1$ is $\Delta C = 0.6258$. This difference decreases as crystal growth progresses, and has become $\Delta C = 0.5789$, 0.4462 and 0.05773 when 30%, 40% and 80% of the crystal has grown, respectively. These ΔC values are smaller than those at the equivalent stages of growth in an axial field because the large vertically downward flow in the parallel layer adjacent to the crystal-melt interface increases lateral uniformity. This lateral segregation is reflected in the constant-concentration curves in the crystal which are presented in Fig. 8.

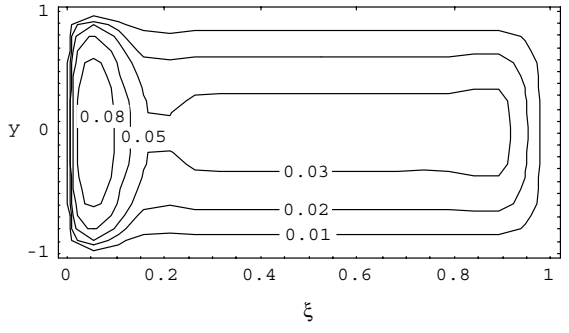

Fig. 6. Contours of the streamfunction in the melt $\psi(\xi, y, t)$ at $t = 0.1264$ for a transverse magnetic field with $B_0 = 2$ T and $C_0 = 0.06$.

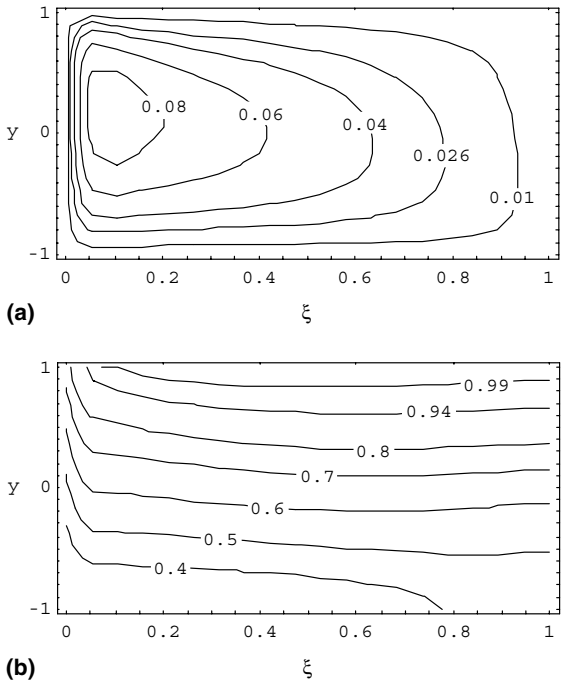

Fig. 7. Contours of the streamfunction and concentration in the melt at $t = 10.11$ for a transverse magnetic field with $B_0 = 2$ T and $C_0 = 0.06$: (a) $\psi(\xi, y, 10.11)$, (b) $C(\xi, y, 10.11)$.

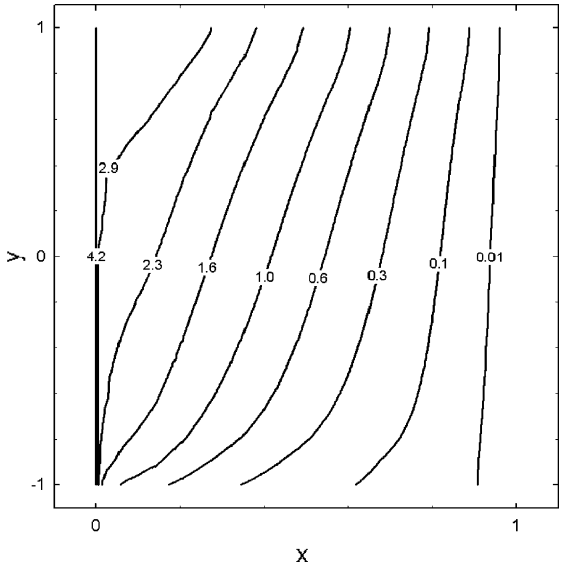

Fig. 8. Contours of the concentration in the crystal $C_s(x, y)$ for a transverse magnetic field with $B_0 = 2$ T, $C_0 = 0.06$, $U_g = 10$ μm/s and $a = 1$.

5. Results for axial segregation in the crystal

The axial variation of the laterally-averaged composition in the crystal is presented in Fig. 9 for the axial field with $B_0 = 2$ T in curve a and the transverse field with $B_0 = 2$ T in curve c. In Fig. 9, we also include the variation for the axial field with $B_0 = 1$ T in curve b and for the transverse field with $B_0 = 1$ T in curve d, and for the well-mixed limit in curve e. Unfortunately, the crystal's concentration continuously decreases along the length of the crystal because of the absorption of the silicon along the crystal-melt interface during growth. Recently, Ma et al. [18] have found that replenishing the melt with fluid having a composition chosen to offset the absorption at the interface can produce a relatively homogeneous crystal. The crystals grown in a transverse magnetic field have steeper slopes for the first-grown part of the crystal. That is, curves c and d for the transverse field have higher crystal concentrations near $x = 0$ than curves a and b for the axial field, respectively. This occurs because the melt in the parallel layer adjacent to the bottom wall at $y = -1$ for the crystal grown in the axial field convects the silicon-depleted melt away from the crystal-melt interface more quickly so that the melt solidifies with higher concentrations at earlier stages of growth. In addition, the crystals grown in a 2 T field solidified with higher concentrations near $x = 0$ than the crystals grown in a 1 T field, as reflected in Fig. 9. The 1 T field provided less electromagnetic damping of the melt motion so that the silicon-depleted melt was convected away from the crystal-melt interface more quickly and the first-grown part of the crystal solidified with lower concentration.

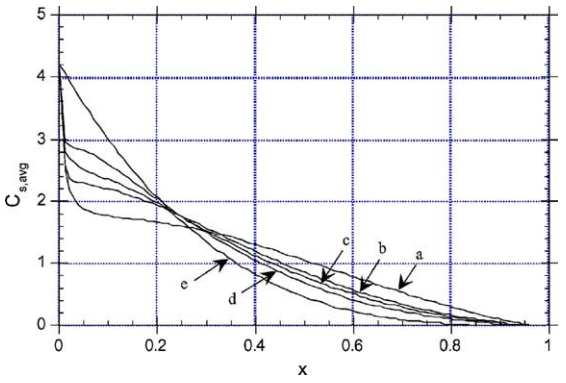

Fig. 9. Axial variation of the laterally-averaged crystal concentration $C_{s,avg}(x)$ with $C_0 = 0.06$, $U_g = 10$ μm/s and $a = 1$ for five cases. *Cases*: (a) axial field with $B_0 = 2$ T, (b) axial field with $B_0 = 1$ T, (c) transverse field with $B_0 = 2$ T, (d) transverse field with $B_0 = 1$ T, and (e) well-mixed limit.

6. Conclusions

During the horizontal Bridgman process where gravity is parallel to the crystal-melt interface, the orientation of the magnetic field has a strong effect on the species transport in the melt. The high-velocity parallel layers are adjacent to the top and bottom walls at $y = \pm 1$ for an axial field while the high-velocity layers are adjacent to the crystal-melt interface and the right end of the container for a transverse magnetic field. A more laterally-uniform crystal can be grown with a transverse magnetic field because the high-velocity parallel layer located adjacent to the crystal-melt interface reduces the lateral segregation. A more axially-uniform crystal can be grown with an axial field with a strong magnetic field.

Acknowledgements

This research was supported by the National Aeronautics and Space Administration under grant NAG8-1817. The calculations were performed on the SGI Origin at the National Center for Supercomputing Applications at the University of Illinois at Urbana-Champaign.

References

[1] M.C. Flemings, Solidification Processing, McGraw-Hill, New York, 1974.
[2] J.I.D. Alexander, J.P. Garandet, J.J. Favier, A. Lizée, g-jitter effects on segregation during directional solidification of tin-bismuth on the MEPHISTO furnace facility, J. Cryst. Growth 178 (1997) 657.
[3] J.P. Garandet, T. Alboussière, in: Modelling and experiments, in: K.W. Benz (Ed.), The Role of Magnetic Fields in Crystal Growth, Progress in Crystal Growth and Characterization of Materials, 38, Elsevier, Amsterdam, 1999, pp. 73–132.
[4] J.S. Walker, in: Models of melt motion, heat transfer and mass transport during crystal growth with strong magnetic fields, in: K.W. Benz (Ed.), The Role of Magnetic Fields in Crystal Growth, Progress in Crystal Growth and Characterization of Materials, 38, Elsevier, Amsterdam, 1999, pp. 195–213.
[5] D.A. Watring, S.L. Lehoczky, Magneto-hydrodynamic damping of convection by an axial magnetic field during vertical Bridgman–Stockbarger growth of HgCdTe, J. Cryst. Growth 167 (1996) 478–487.
[6] N. Ramachandran, D.A. Watring, Convection damping by an axial magnetic field during growth of HgCdTe by vertical Bridgman method—thermal effects, AIAA 35th Aerospace Sciences Meeting and Exhibit, Reno, NV, AIAA Paper #97-0450 (1997).
[7] J.P. Garandet, T. Alboussière, R. Moreau, Buoyancy driven convection in a rectangular enclosure with a

transverse magnetic field, Int. J. Heat Mass Transfer 35 (1992) 741–748.
[8] M.V. Farrell, N. Ma, Coupling of buoyant convections in boron oxide and a molten semiconductor in a vertical magnetic field, J. Heat Transfer 124 (2002) 643–649.
[9] J.M. Hirtz, N. Ma, Dopant transport during semiconductor crystal growth. Axial versus transverse magnetic fields, J. Cryst. Growth 210 (2000) 554–572.
[10] J.E. Hart, On sideways diffusive stability, J. Fluids Mech. 49 (1971) 279–288.
[11] N. Ma, Solutal convection during growth of alloyed semiconductor crystals in a magnetic field, J. Thermophys. Heat Transfer 17 (2003) 77.
[12] D.H. Matthiesen, M.J. Wargo, S. Motakef, D.J. Carlson, J.S. Nakos, A.F. Witt, Dopant segregation during vertical Bridgman–Stockbarger growth with melt stabilization by strong magnetic fields, J. Cryst. Growth 85 (1987) 557–560.
[13] N. Ma, J.S. Walker, Inertia and thermal convection during crystal growth with a steady magnetic field, J. Thermophys. Heat Transfer 15 (2001) 50–54.
[14] N. Ma, J.S. Walker, Dopant transport during semiconductor crystal growth with magnetically damped buoyant convection, J. Cryst. Growth 172 (1997) 124–135.
[15] Y.M. Gelfgat, L.A. Gorbunov, An additional source of force convection in semiconductor melts during single-crystal growth in magnetic fields, Soviet Phys. Doklady 34 (1989) 470–473.
[16] L.D. Landau, E.M. Lifshitz, Electrodynamics of Continuous Media, Pergamon Press Ltd, New York, 1984.
[17] R.W. Olesinski, G.J. Abbaschian, The Ge–Si (germanium-silicon) system, Bulletin of Binary Phase Diagrams 5 (1984) 180–183.
[18] N. Ma, D.F. Bliss, G.W. Iseler, Vertical gradient freezing of doped gallium–antimonide semiconductor crystals using submerged heater growth and electromagnetic stirring, J. Cryst. Growth 259 (2003) 26–35.